Received 6 August 2022; revised 31 August 2022; accepted 6 September 2022. Date of publication 13 September 2022; date of current version 26 September 2022.

Digital Object Identifier 10.1109/OJCOMS.2022.3205346

Optimization of the Exponential Bounds on the Gaussian *Q* Function Using Interior Point Algorithm and Its Application in Communication Theory

ADITYA POWARI[1], DHARMENDRA SADHWANI[1], LALITA GUPTA[2] (Senior Member, IEEE), AND RAM NARAYAN YADAV[2]

[1]Department of Electrical and Computer Science Engineering, Institute of Infrastructure Technology Research and Management, Ahmedabad 380026, India

[2]Department of Electronics and Communication Engineering, Maulana Azad National Institute of Technology, Bhopal 462003, India

CORRESPONDING AUTHOR: D. SADHWANI (e-mail: dharmendrasadhwani@gmail.com)

ABSTRACT Owing to various applications in the field of wireless communication systems, in this paper, using vector-based interior-point algorithm, we propose a generic methodology which optimizes simple exponential based approximations of the Gaussian Q function (GQF) yielding extremely accurate optimized approximations. We optimize the relative error (RE) which is considered as one of the key metrics used to evaluate the performance of these approximations. Precisely, we target the points of *local maximas* where the RE is high, defining a new set of optimized coefficients yielding reduced RE at these points of concern. We also optimize the points of *local minimas*; however at these points the percentage reduction in RE is not that significant. We then compute the harmonic mean of all these optimal coefficients which makes the originally proposed bounds much tighter, for the entire performance range of the GQF. We further illustrate the tightness of the optimized approximation by facilitating the accurate computation of the error performance metrics like symbol error probability of various coherent digital modulation schemes like square quadrature amplitude modulation (SQAM), rectangular-QAM, cross-QAM and hexagonal-QAM over the versatile $\kappa-\mu$ shadowed fading channel. The analysis is also validated with the help of Monte-Carlo simulations.

INDEX TERMS Optimization, vector-based interior-point algorithm, Gaussian Q function, $\kappa-\mu$ shadowed fading channel, digital modulation techniques, wireless communication systems, approximate computing.

I. INTRODUCTION

THE GAUSSIAN Q function (GQF) defined as

$$Q(x)=\frac{1}{\sqrt{2\pi}}\int_{x}^{\infty}\exp\left(-\frac{u^2}{2}\right)du, \tag{1}$$

plays a vital role in computation of the bit-error-rate (BER) of several wireless communication systems in the presence of additive white Gaussian noise (AWGN) and multi-path fading [1]. However, the form given in (1) is not convenient to work with and hence it becomes essential to look for some alternatives which makes (1) tractable without losing its accuracy.

To meet these challenges, several approximations of the GQF have been proposed in the open literature [2], [3], [4], [5], [6], [7], [8], [9], [10], [11], [12], [13], [14], [15]; which prove to be significant in a variety of applications. For example, the authors in [2, eq. (8)] first proposed an exponential based approximation for the GQF; and ever since its inception, it became very popular as it facilitates the BER for various systems like non-orthogonal multiple access (NOMA)-based Internet of Things (IoT) networks [16], visible light communication (VLC) systems [17], multiple-input-multiple-output (MIMO) systems with widely linear minimum mean square error (WLMMSE) receiver [18], sparse layered MIMO systems [19], systems employing convolution neural network (CNN) as posterior classifier [20]; and large intelligent surface (LIS) based generalized spatial modulation (GSM) systems [21], [22]. Similarly, the Prony-approximation derived in [3] is used to evaluate the BER of index-modulation (IM)-aided orthogonal frequency division multiplexing (OFDM) systems [23]. Noteworthy, IM is a technique which is widely used in fifth-generation (5G)

This work is licensed under a Creative Commons Attribution 4.0 License. For more information, see https://creativecommons.org/licenses/by/4.0/

networks to meet the demand of high throughput and low energy consumption; satisfying the ever growing demands of future IoT [24]. Moreover, the Prony-approximation finds its utility in performance analysis of various other wireless communication systems like decode-and-forward (DF) cooperative systems [25], two-way satellite relaying with estimated channel gains [26], free space optical (FSO) communication systems [27], systems with orthogonal space time block codes (OSTBC) [28], [29], imperfect feedback-based linear precoding schemes for MIMO systems [30]; and reconfigurable intelligent surface (RIS)-aided dual-hop mixed radio frequency (RF)-FSO communication systems [31], [32]. In the same way, the very popular Karagiannidis and Lioumpas (KL) approximation [4] finds its utility in the performance analysis of energy-efficient MIMO-OFDM systems [33] and coherently distributed systems employing direction of arrival (DOA) estimation [34].

Apart from all the aforementioned applications, the approximations of the GQF facilitate the symbol error probability (SEP) computation of various coherent digital modulation schemes like square quadrature amplitude modulation (SQAM), rectangular-QAM (RQAM), cross-QAM (XQAM) and hexagonal-QAM (HQAM) over AWGN and various fading statistics. For example, the trapezoidal based approximation [10] facilitates the SEP of the aforementioned digital modulation techniques over $\kappa - \mu$ shadowed fading channel [35]. Similarly, leveraging the trapezoidal numerical integration method, the authors in [36] proposed tight approximations of the SEP of M-Ary phase-shift-keying over $\kappa - \mu$ shadowed fading channel. Noteworthy, it is essential to accurately compute the error performance of these digital modulation techniques as they are widely used in several emerging areas of communications [37] which require high transmission data rate like optical wireless communications (OWC), fifth-generation (5G) communications, energy-constrained communication systems. To achieve this, the approximations of the GQF play a vital role.

Hence, looking at the diverse applications of the approximations of the GQF particularly in the field of wireless communication systems, it is imperative to improve the accuracy of the same. As an instance, the first exponential based approximation given by the authors in [2, Eq. (8)] is not accurate enough particularly for the lower values of x. Since then, improving the accuracy of the GQF has been quite a challenging area for the potential researchers without compromising on its tractability but it has been seen that there is always a trade-off between the accuracy and tractability of an approximation. For example, the KL approximation [4] is fairly accurate but due to the presence of the combination of algebraic and exponential functions, it is cumbersome to compute. To a certain extent, the intractability of [4] has been tackled in [6] where the Taylor series expansion of one of the exponential terms of [4] has been carried out which is then truncated to a finite number of terms till a sufficient level of the accuracy is achieved. However, since [6] is further an approximated version of [4], it is not accurate enough, and a large number of terms are needed if we want to achieve some amount of accuracy; which increases the complexity of the approximation. Moreover, it should also be noted that if an approximation performs well for one particular range of x, it may happen that it does not give the desired results for the other values of x. This limits the usefulness of an approximation for a wider range of x.

Hence, to yield accurate results for a considerable range of x, the optimization process proves to be significant. For example, using several non-linear equations, the authors in [11] tried to optimize an already existing exponential based approximation [2, (8)] with a challenge of minimizing the absolute error (AE) and the relative error (RE); but the optimization did not yield the desired results as one can achieve better AE or RE at the cost of the other. This dilutes the significance of [11] as the optimized coefficients are not generic in nature, i.e., they do not perform well for both the types of errors. Moreover, the authors in [11] have clearly stated that the error function needs to be reshaped if there is a need of the improvement of accuracy over a specified range of x; but at the same time this results in the loss of accuracy for the other ranges of x. This again provides an insight that the performance of [11] is limited to only one particular range of x. Moreover, the presence of non-linear equations in [11] increases the computational complexity of the optimization process. Similarly, the authors in [38] optimized the AE of [2, (8)] via Remez exchange algorithm and derived the optimized coefficients enhancing the accuracy of [2]. However, the work of [38] is limited to the optimization of AE only. Further, the authors in [10] proposed tighter trapezoidal based approximations with three and four number of simple exponential terms. However, if we see the complete range of x, it does not yield desired results particularly for very low ($x \leq 0.5$) and high values of x ($x \geq 3$).

This motivates to look for a methodology which optimizes an already existing simple exponential based approximation which the challenges of improving its accuracy for the entire range of x; without compromising on its tractability. To meet these challenges, in this paper, we develop a generic optimization methodology which can be used to improve the accuracy of all the approximations as long as the GQF is expressed in terms of the sum of simple exponentials only. To show the utility of the proposed method, as an instance, we explore the exponential bounds given by the authors in [3]; rest all other bounds/approximations can be similarly optimized by the potential researchers. To do so, we implement the vector-based interior-point algorithm (IPA) which is used to optimize any linear cost function. In this paper, this cost function is the RE expression. We highlight some characteristics owing to which the RE performance of the bounds of [3] is not accurate enough at various *local maximas* of the corresponding RE plot. The objective of this paper is to optimize the RE expression at these points of concern eventually providing the new optimized coefficients. We

derive the optimal coefficients corresponding to the points of *local minimas* as well. We further compute the harmonic mean (HM) of these optimal coefficients which enhances the accuracy of the original approximation [3] for a considerable performance range of the GQF. To the best of authors' knowledge, vector-based IPA used to optimize any linear GQF approximation is not reported in the literature before. We further show the significance of the optimized approximation to compute the SEP of coherent digital modulation techniques over the versatile $\kappa-\mu$ shadowed fading channel. Noteworthy, apart from including all the popular fading channels like Rayleigh, Nakagami-*m*, $\eta-\mu$, $\kappa-\mu$ etc. as its special cases, the $\kappa-\mu$ shadowed fading channel is used in a variety of applications [39], [40], [41], [42], [43], [44], [45], [46], [47], [48], [49], [50], [51].

The remainder of the paper is organized as follows: Section II provides the motivation needed for the research formulation. Section III gives a detailed mathematical background on the vector-based IPA which is used to optimize the points of *local maximas* and *local minimas*. Section III-A gives an insight on the newly derived coefficients using IPA. Section III-B shows the application of the new optimized approximation in error performance analysis of various coherent digital modulation schemes over $\kappa-\mu$ fading channel. Concluding remarks is given in Section IV which is followed by the Appendices 'A' and 'B'.

II. MOTIVATION AND PROBLEM STATEMENT

In this paper, we explicitly demonstrate the working of IPA to optimize the approximation of the complementary error function, $erfc(x)$, with two ($p=2$) and three ($p=3$) number of terms [3]. These are respectively given as

$$F(x) \approx 0.416e^{-1.942x^2} + 0.294e^{-1.05x^2} \tag{2a}$$

and

$$F(x) \approx 0.336e^{-1.752x^2} + 0.288e^{-1.05x^2} + 0.004e^{-1.206x^2}. \tag{2b}$$

Fig. 1 provides an insight on the performance of (2) by showing the presence of several *local maximas* in the RE curve of (2). The RE is defined as:

$$RE = \frac{|erfc(x) - F(x)|}{erfc(x)} \times 100. \tag{3}$$

It can be inferred from the figure that the original coefficients of (2) viz. [0.416, 0.294] for $p=2$ and [0.336, 0.288, 0.004] for $p=3$ are not performing well at the *local maximas*; as the RE is quite high at these points.

Table 1 further provides an insight on the performance of (2) at the points of *local maximas* by comparing (2) with the actual $erfc(x)$ function in terms of the percentage RE. It is quite evident that the RE is comparatively high at these points. Furthermore, as seen from Fig. 1, the regions lying in the neighbourhood of these *local maximas* also have sufficiently high RE. Noteworthy, the regions around *local minimas* that occur in the RE curve signifies those regions where the original set of coefficients are working fine as

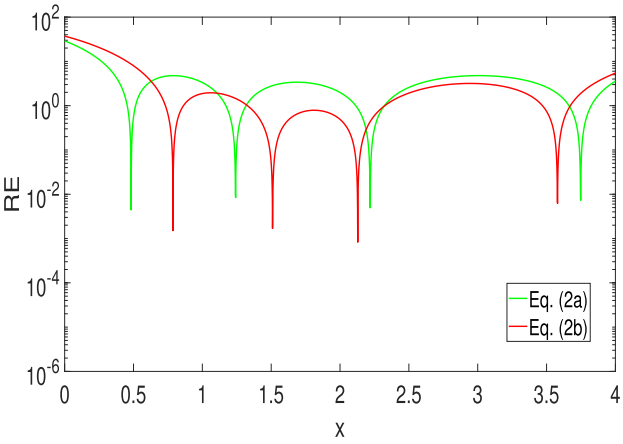

FIGURE 1. RE Plot for original prony p=2,3 approximation (2).

TABLE 1. Local maximas and corresponding RE for (2).

For Eq. (2a)			
Local Maxima (x)	$erfc(x)$	$F(x)$	RE (%)
0	1.0000	0.7100	29.0000
0.7908	0.2634	0.2760	4.7651
1.6870	0.0170	0.0165	3.3906
3.0074	2.1083e-05	2.2089e-05	4.7759
For Eq. (2b)			
Local Maxima (x)	$erfc(x)$	$F(x)$	RE (%)
0	1.0000	0.6280	37.2000
1.0609	0.1335	0.1361	1.9549
1.8119	0.0104	0.0103	0.7880
2.9440	3.1348e-05	3.2345e-05	3.1793

it can be seen that the RE is getting reduced in those regions. However, the rate at which these *local minimas* appear is quite low which implies that the coefficients of (2) are not accurate enough for quite a considerable range of x.

The problem is not just limited to (2), i.e., one can find several other similar exponential based approximations viz [2], [5], [10], [11], [12], [13] where one can find several *local maximas* in the corresponding RE plots. Hence, it is imperative to improve the accuracy of all such approximations for a considerable range of x. In this paper, we explicitly optimize (2) whereas for the other aforementioned approximations, a similar procedure can be adopted. Noteworthy, just by making use of *max* and *min* functions in the *MATLAB* software, one can easily compute the corresponding maximum and minimum values in an array along with their index locations. This method can be summarized as:

- Plot the RE (3) curve corresponding to any linear exponential based approximation as stated above over the range of $x \in [0, 4]$.
- Identify the sub-ranges over which one can find a *local maxima* or a *local minima*.
- Over a sub-range, run the *max* or *min* function accordingly to obtain the RE values at *local maximas* and *minimas* along with their corresponding location of x.

We would also like to highlight that the since the location of *local maximas* and *local minimas* is independent of time, i.e.,

the RE is only the function of x and not the function of time, the location of these points of concern will not change and therefore this problem statement and the solution proposed below are very much useful for a realistic system.

III. VECTOR-BASED IPA

In this section, we optimize a linear cost function $f(x)$ for n number of variables $(x_1, x_2, \ldots, x_n)$ as:

$$\min f(X) = C^T X_{n\times 1}. \tag{4}$$

Noteworthy, Eq. (4) is subjected to constraints

$$A_{m\times n} X_{n\times 1} = B_{m\times 1}, \tag{5}$$

where $X = \begin{bmatrix} x_1 \\ x_2 \\ \cdot \\ \cdot \\ \cdot \\ x_n \end{bmatrix}$ such that $x_j \geq 0; \forall j \in [1, n]$,

$C^T = \begin{bmatrix} c_1 & c_2 & \cdot & \cdot & \cdot & c_n \end{bmatrix}$ and A, B matrices basically compose of the coefficients present in the given constraint conditions to the said problem.

Let $X^{(0)}_{n\times 1}$ be an initial vector composing of the variables which are of the form of $x_j^{(0)}$, $\forall\ j \in [1, n]$, such that all of them lie inside a Feasible Region (FR). This FR is determined by the inequality constraints which can be easily converted into the corresponding equality constraints by simply incorporating a *slack variable*.

In order to ensure the best performance of IPA, it is imperative that the input data point must be centered, i.e., it must be equidistant from all the n axis defining the FR. Hence, we need to scale this $X^{(0)}_{n\times 1}$ vector into a new vector say $Y^{(0)}_{n\times 1}$ such that this criterion is met. To facilitate this mechanism, we now define a scaling matrix (S) as:

$$X^{(0)} = SY^{(0)}, \tag{6}$$

where

$$S = \begin{bmatrix} x_1^{(0)} & & & & \\ & x_2^{(0)} & & & \\ & & \cdot & & \\ & & & \cdot & \\ & & & & \cdot \\ & & & & & x_n^{(0)} \end{bmatrix}$$

is $n \times n$ Diagonal matrix. It is to be noted that the diagonal elements of this matrix are basically just the contents of $X^{(0)}$.

From (6), we can write $Y^{(0)} = S^{-1}X^{(0)}$ where

$$S^{-1} = \begin{bmatrix} \frac{1}{x_1^{(0)}} & & & & \\ & \frac{1}{x_2^{(0)}} & & & \\ & & \cdot & & \\ & & & \cdot & \\ & & & & \cdot \\ & & & & & \frac{1}{x_n^{(0)}} \end{bmatrix},$$

yielding the vector $Y^{(0)} = \begin{bmatrix} 1 \\ 1 \\ \cdot \\ \cdot \\ \cdot \\ 1 \end{bmatrix}$.

Note that all the elements of $Y^{(0)}$ are equal which signifies that the data point resembled by vector $Y^{(0)}$ in the FR is equidistant from all the n axis. Now according to the transformation $X = SY$, we define the scaled linear optimization problem in terms of the vector Y having n variables viz. $(y_1, y_2, \ldots, y_n)$ by respectively modifying (4) and (5) as:

$$\min f(Y) = P^T Y_{n\times 1}, \tag{7}$$

and

$$K_{m\times n} Y_{n\times 1} = B_{m\times 1}, \tag{8}$$

where $P = CS$ and $K_{m\times n} = A_{m\times n} S_{n\times n}$. For vector Y, here as well we will have $y_j \geq 0; \forall j \in [1, n]$ in accordance with the original problem statement.

In order to start the optimization process using IPA, our next objectives are to find a suitable direction vector (descent direction), $D_{n\times 1}$, and step size λ; computing a new data point $Y^{(1)}$ as

$$Y^{(1)} = Y^{(0)} + \lambda D. \tag{9}$$

To accomplish the aforementioned objectives, we first define the projection matrix, $H_{n\times n}$, as

$$H = I - K^T\left(KK^T\right)^{-1}K, \tag{10}$$

where I is an $n \times n$ identity matrix. This H matrix satisfies the following two properties:

$$H^T = H \tag{11a}$$

and

$$H^2 = H. \tag{11b}$$

It should be noted that these properties can be easily derived from (10).

The following *Lemmas* will ensure that the objectives as stated above are met:

Lemma 1: The direction vector $D_{n\times 1}$ is defined as

$$D = -HP. \tag{12}$$

Proof: See Appendix A. ■

Lemma 2: The step size is defined as $\lambda = 0.9 \times \lambda_{max}$, where

$$\lambda_{max} = \min_{\forall d_j < 0} \left\{ \frac{y_j^{(0)}}{-d_j} \right\},$$

y_j and d_j are the j^{th} elements of the Y and D vectors respectively.

Proof: See Appendix B. ■

Hence, as these objectives corresponding to the choices of λ and D are met, we can find out the next data point

Algorithm 1 Vector-Based IPA

1: Determine $X^{(0)}$, C^T, A, B.
2: **repeat**
3: Formulate S and scale the problem
4: Determine scaled problem matrices P, K
5: Determine H and set $D = -HP$
6: Determine λ_{max} and set $\lambda = 0.9 \times \lambda_{max}$
7: Obtain the new scaled data point vector Y.
8: Use S to descale it into X.
9: Compute the cost function value $f(X)$
10: **until** $f(X^{(j)}) - f(X^{(j+1)}) < 10^{-6}$

TABLE 2. Mean optimal coefficients of (14).

α_{Mopt}	0.428584327960569
β_{Mopt}	0.303629267990350
α'_{Mopt}	0.347467003877914
β'_{Mopt}	0.297744033685541
ζ'_{Mopt}	0.001436242987287

$(Y^{(1)})$ which lies in the interior of the FR, as defined in (9). Afterwards, we make use of (6) to get the corresponding $X^{(1)}$ vector for our original problem statement and using that we can compute our cost function value $f(X^{(1)})$. Similarly to get the next data point $X^{(2)}$ we again need to define the scaling matrix but this time with the contents of $X^{(1)}$ and repeat the entire procedure again to obtain $X^{(2)}$ data point. This process is repeated till the time an optimal solution is reached. Lastly, we define the criteria to terminate the IPA implying that the optimal solution has been obtained. For any j^{th} iteration and the next $(j+1)^{th}$ iteration if:

$$f\left(X^{(j)}\right) - f\left(X^{(j+1)}\right) < 10^{-6} \tag{13}$$

holds true then we conclude that an optimal solution has been obtained and the IPA is terminated.

The aforementioned algorithm can be summarized by the following flow-chart.

A. NEW OPTIMIZED COEFFICIENTS USING IPA

Proposition 1: Using IPA, via Table 2, we now propose new mean optimal coefficients in replacement of the original coefficients of (2a) and (2b) denoted by α_{Mopt}, β_{Mopt} for $p = 2$ and α'_{Mopt}, β'_{Mopt}, ζ'_{Mopt} for $p = 3$. This gives rise to the novel optimized approximations given as

$$F_{Mopt}(x) \approx \alpha_{Mopt} e^{-1.942x^2} + \beta_{Mopt} e^{-1.05x^2} \tag{14a}$$

and

$$F_{Mopt}(x) \approx \alpha'_{Mopt} e^{-1.752x^2} + \beta'_{Mopt} e^{-1.05x^2} + \zeta'_{Mopt} e^{-1.206x^2}. \tag{14b}$$

Proof: We first define the optimized approximations corresponding to the *local maximas* and *local minimas* in the RE curve of (2). These are given as

$$F_{opt}(x) \approx \alpha e^{-1.942x^2} + \beta e^{-1.05x^2} \tag{15a}$$

and

$$F_{opt}(x) \approx \alpha' e^{-1.752x^2} + \beta' e^{-1.05x^2} + \zeta' e^{-1.206x^2}, \tag{15b}$$

where α, β, α', β', ζ' are the optimized coefficients corresponding to the *local maximas* and *local minimas*. ■

Precisely, we first optimize the RE (as defined in Eq. (3)) to get the values of the aforementioned coefficients. For that, we take (15a) and define our problem statement as

$$\min f(X) = \left|1 - \alpha \frac{e^{-1.942x^2}}{erfc(x)} - \beta \frac{e^{-1.05x^2}}{erfc(x)}\right|. \tag{16}$$

For a definite input value of x (which is a *local maxima* or a *local minima*), the fractional terms associated with the coefficients in (16) will result into some constant values. So we can rewrite (16) as:

$$\min f(X) = |1 - c_1\alpha - c_2\beta|$$

or equivalently,

$$\min f(X) = |c_1\alpha + c_2\beta - 1|.$$

This can be expressed in a linear form as described in (4) where,

$$C^T = \begin{bmatrix} c_1 & c_2 & -1 \end{bmatrix}$$

and

$$X = \begin{bmatrix} \alpha \\ \beta \\ 1 \end{bmatrix}.$$

Furthermore, in (15a) when $x = 0$ we get,

$$F_{opt}(x) = \alpha + \beta$$

Now since $erfc(0) = 1$, it is imperative that for $x = 0$ we should have $\alpha + \beta = 1$. Since for $x \geq 0$, $erfc(x)$ is essentially a monotonically decreasing function, the inequality constraint for our problem can be formulated as $\alpha + \beta \leq 1$, where $\alpha \geq 0$ and $\beta \geq 0$. In order to facilitate the IPA, we convert this inequality constraint into an equality constraint by means of a *slack* variable ψ, which we will incorporate in the initial vector $X^{(0)}$. Thus, we can write the corresponding equality constraint as

$$\alpha + \beta + \psi = 1. \tag{17}$$

The input matrices corresponding to (17) are $A = \begin{bmatrix} 1 & 1 & 1 \end{bmatrix}$ and $B = [1]$. The initial input vector $X^{(0)}$ is formed by taking the original values of α and β in (2a), i.e., 0.416 and 0.294 respectively. Substituting these values in (17), the initial value of ψ comes out to be $1 - 0.416 - 0.294 = 0.290$, yielding

$$X^{(0)} = \begin{bmatrix} 0.416 \\ 0.294 \\ 0.290 \end{bmatrix}.$$

Now by taking the definite value of x as an input, the constants c_1, c_2 are determined and C^T vector is formulated. Noteworthy, the factors that are in the exponents of (2) are

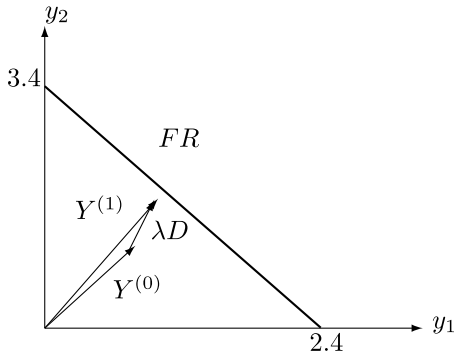

FIGURE 2. Illustration of the feasible region, initial point, new point, direction vector and step size.

TABLE 3. Demonstration of RE reduction (convergence) at local maxima and minima.

Maxima $x = 0$	
No. of Iterations	RE
0	2.900000e-01
1	1.995455e-01
2	3.848716e-02
3	3.553322e-02
4	1.002357e-02
5	6.749971e-03
6	4.598944e-04
7	1.125638e-04
8	7.667683e-05
9	1.518130e-06
10	2.783929e-07
11	5.151543e-09
Minima $x = 3.7473$	
No. of Iterations	RE
0	3.197444e-06
1	1.705897e-07
2	2.119954e-08

used in determining C^T. Furthermore, here, in order to center the data the Scaling matrix will be

$$S = \begin{bmatrix} 0.416 & 0 & 0 \\ 0 & 0.294 & 0 \\ 0 & 0 & 0.290 \end{bmatrix}.$$

Using this, we write the scaled inequality constraint as $0.416y_1 + 0.294y_2 \leq 1$. This inequality governs the FR of the optimization process. Graphically, this FR is the interior of the triangle which is formed by the two axis and the constraint line, as shown in Fig. 2.

Now IPA carries out the optimization process and we eventually obtain the optimized coefficients α, β for an input x when the termination criteria (13) is satisfied. A similar approach can be used for (15b) in order to obtain α', β', ζ'.

Table 3 demonstrates the convergence of IPA for optimization of (2a) at *maxima* $x = 0$ and *minima* $x = 3.7473$. As expected, the successive values of the cost function (RE) decrease over iterations and we can see that IPA eventually terminates once the termination criteria (13) is met. In this way, we not only optimized the points of *local maximas* where the RE is high but the points of *local minimas* as well. In Tables 4 and 5 we have listed the

TABLE 4. Optimized coefficients for eq. (15a).

Local Maxima and corresponding optimized coefficients		
Point	α	β
Max 1	0.560999997424228	0.438999997424228
Max 2	0.405564389756889	0.275770327329548
Max 3	0.416900341533637	0.305400111908863
Max 4	0.415995919283067	0.280592886317516
Local Minima and corresponding optimized coefficients		
Point	α	β
Min 1	0.415995986230111	0.293995054350054
Min 2	0.416000167385373	0.293997925424583
Min 3	0.415999998722261	0.293999894640623
Min 4	0.416009941301644	0.293999053681008

TABLE 5. Optimized coefficients for eq. (15b).

Local Maxima and corresponding optimized coefficients			
Point	α'	β'	ζ'
Max $1'$	0.459999997973442	0.411999997973442	0.12799997973442 00
Max $2'$	0.333977921218506	0.283544054141979	0.00026162744078957
Max $3'$	0.336187557836942	0.289879449062907	0.00512617452083789
Max $4'$	0.335980934782084	0.279630505557138	0.00183477030289134
Local Minima and corresponding optimized coefficients			
Point	α'	β'	ζ'
Min $1'$	0.336000551828221	0.288000853695572	0.00400077387649081
Min $2'$	0.336000037050779	0.288000183707279	0.00400013671914886
Min $3'$	0.336000016867208	0.288000255853544	0.00400015315612890
Min $4'$	0.336000002413347	0.287998989555026	0.00399986457777553

TABLE 6. Illustration of local maxima optimization for (15).

For Eq. (15a)				
Point	x	$erfc(x)$	$F_{opt}(x)$	$\text{RE}_{opt}(\%)$
Max 1	0	1.0000	1.0000	5.1515e-07
Max 2	0.7908	0.2634	0.2634	4.9181e-08
Max 3	1.6870	0.0170	0.0170	1.2146e-06
Max 4	3.0074	2.1083e-05	2.1083e-05	1.0668e-06
For Eq. (15b)				
Point	x	$erfc(x)$	$F_{opt}(x)$	$\text{RE}_{opt}(\%)$
Max $1'$	0	1.0000	1.0000	6.0797e-07
Max $2'$	1.0609	0.1335	0.1335	4.0819e-07
Max $3'$	1.8119	0.0104	0.0104	8.6875e-07
Max $4'$	2.9440	3.1348e-05	3.1348e-05	1.0715e-07

TABLE 7. Accuracy comparison of original (2) and optimized (15) at local minimas.

Comparison of (2a) and (15a)			
Point	x	RE(%)	$\text{RE}_{opt}(\%)$
Min 1	0.4830	0.0013	3.8586e-08
Min 2	1.2411	5.0887e-04	9.4096e-08
Min 3	2.2189	3.2865e-05	2.3595e-06
Min 4	3.7473	3.1974e-04	2.1199e-06
Comparison of (2b) and (15b)			
Point	x	RE(%)	$\text{RE}_{opt}(\%)$
Min $1'$	0.7870	3.7670e-04	8.7681e-07
Min $2'$	1.5102	8.0097e-05	6.5872e-08
Min $3'$	2.1285	1.1108e-04	1.8159e-06
Min $4'$	3.5792	3.5425e-04	2.2468e-06

local maximas and *local minimas* along with the corresponding optimized coefficients. Using the optimized coefficients, Tables 6 and 7 further illustrate the results obtained via optimization of the *local maximas* and *local minimas*.

After obtaining the optimal coefficients of (15), we take their harmonic mean (HM) which eventually computes the mean optimal coefficients, as listed in Table 2. This facilitates the optimization of the original approximation (2)

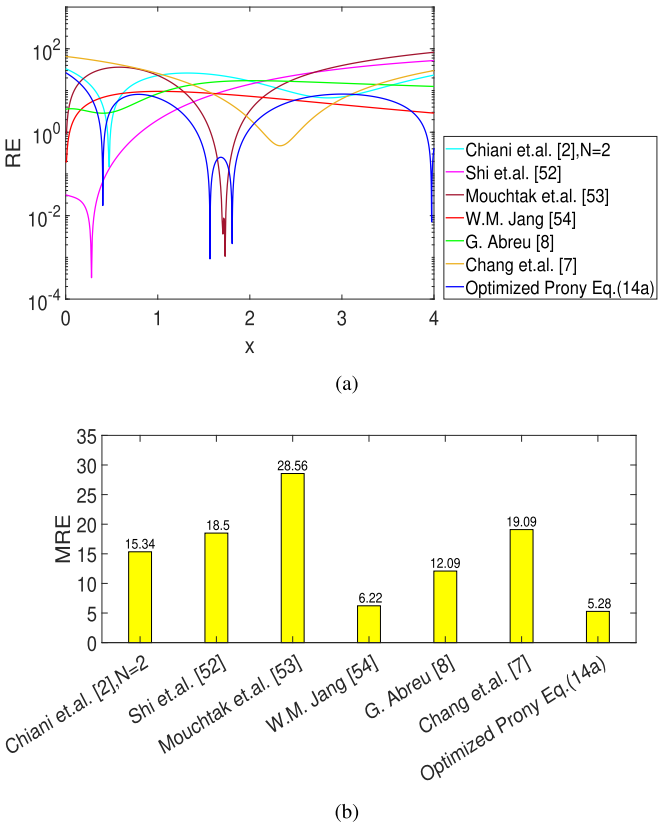

FIGURE 3. Relative error comparison of the optimized approximation (14a) with existing well-known approximations viz [2], [8], [52], [53], [54] and [7].

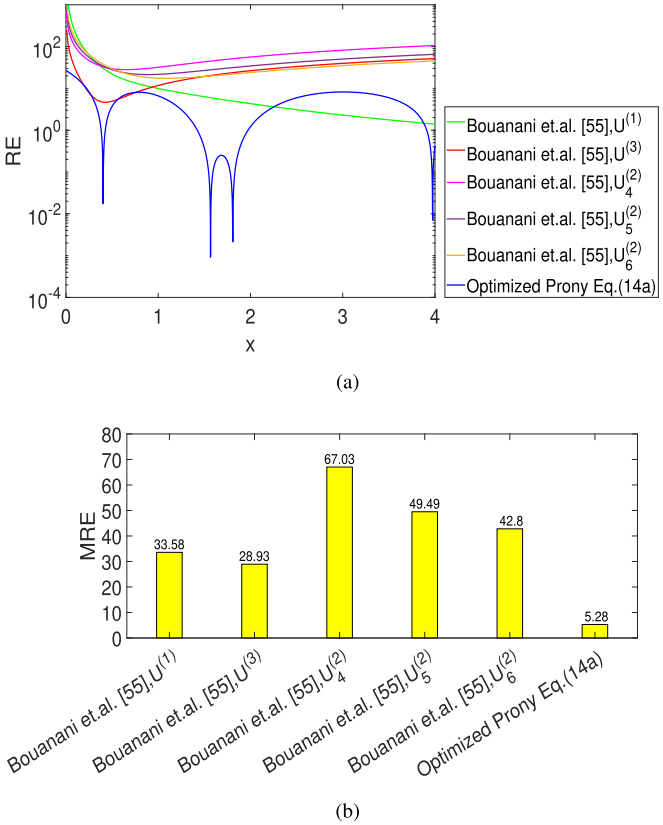

FIGURE 4. Relative error comparison of the optimized approximation (14a) with popular bounds on the Gaussian *Q* function [55].

over the entire range of x; thereby completing the proof of (14).

Fig. 3 shows the significance of the proposed optimized approximation (14a) over other existing well-known approximations/bounds available in the open literature [2], [7], [8], [52], [53], [54]. It can be clearly seen that the mean relative error (MRE) of (14a) is least (5.28%) among all the aforementioned approximations thereby providing an insight on its accuracy. Fig. 4 further compares the proposed work with the bounds of [55]. Here also, in terms of accuracy, Eq. (14a) supersedes all these bounds.

B. APPLICATIONS OF THE OPTIMIZED APPROXIMATION (14) IN ERROR PERFORMANCE OF VARIOUS DIGITAL MODULATION SCHEMES OVER THE VERSATILE $\kappa-\mu$ SHADOWED FADING CHANNEL

The proposed optimized approximation (14) finds its utility in the SEP computation of various coherent digital modulation schemes over fading statistics. In the following proposition, we propose the SEP of widely used digital modulation scheme viz. $M-$Ary SQAM [1] over the versatile $\kappa-\mu$ shadowed fading channel [58].

Proposition 2:

$$P_{fading} \approx A_1 \sum_{i=1}^{2} \delta_i M_\gamma\left(-\theta_i \sigma^2\right) - A_2 \sum_{i=1}^{3} \delta_i' M_\gamma\left(-\theta_i' \sigma^2\right) \tag{18}$$

where $A_1, A_2, \delta_i, \theta_i, \sigma_i, \delta_i', \theta_i'$ are defined in Table 8; and $M_\gamma(\cdot)$ is the moment generating function (MGF) of the $\kappa-\mu$ shadowed fading channel.

Proof: The general expression to compute the SEP of coherent digital modulation techniques over $\kappa-\mu$ shadowed fading channel is given as

$$P_{fading} = \int_0^\infty P_{AWGN} p_\gamma(\gamma) d\gamma, \tag{19}$$

where P_{AWGN} is the SEP expressions of various coherent digital modulation schemes over AWGN channel, as listed in Table 8; and $p_\gamma(\gamma)$ is the PDF of the $\kappa-\mu$ shadowed fading channel given as [58].

$$p_\gamma(\gamma) = \frac{\mu^\mu m^m (1+\kappa)^\mu}{\Gamma(\mu)\bar{\gamma}(\mu\kappa+m)^m}\left(\frac{\gamma}{\bar{\gamma}}\right)^{\mu-1} \times e^{-\frac{\mu(1+\kappa)\gamma}{\bar{\gamma}}} \times {}_1F_1\left(m, \mu; \frac{\mu^2\kappa(1+\kappa)}{\mu\kappa+m}\frac{\gamma}{\bar{\gamma}}\right), \tag{20}$$

where γ is the instantaneous signal to noise ratio (SNR), $\bar{\gamma}$ is the average SNR, $\kappa \geq 0$, $\mu > 0$, $0.5 \leq m < \infty$ are the fading parameters, $\Gamma(\cdot)$ is the gamma function [59, (8.310/1)], ${}_1F_1$ is the confluent hypergeometric function [59, (9.210/1)] and s is a constant. ■

TABLE 8. Modulation schemes and their SEP expressions in AWGN and $\kappa-\mu$ shadowed fading channel.

Modulation Scheme	SEP in AWGN Channel	SEP in $\kappa-\mu$ Shadowed Fading Channel
$M-$SQAM [1]	$P_{AWGN}=A_1Q(\sigma\sqrt{\gamma})-A_2Q^2(\sigma\sqrt{\gamma})$	$P_{fading}\approx A_1\sum_{i=1}^{2}\delta_i M_\gamma(-\theta_i\sigma^2)-A_2\sum_{i=1}^{3}\delta_i' M_\gamma(-\theta_i'\sigma^2)$
$M\times N-$RQAM [1]	$P_{AWGN}=B_1Q(\psi\sqrt{\gamma})-B_2Q^2(\psi\sqrt{\gamma})$	$P_{fading}\approx B_1\sum_{i=1}^{2}\delta_i M_\gamma(-\theta_i\psi^2)-B_2\sum_{i=1}^{3}\delta_i' M_\gamma(-\theta_i'\psi^2)$
$M\times N-$XQAM [56]	$P_s\approx C_1Q(\tau\sqrt{\gamma})-C_2Q^2(\tau\sqrt{\gamma})$	$P_{fading}\approx C_1\sum_{i=1}^{2}\delta_i M_\gamma(-\theta_i\tau^2)-C_2\sum_{i=1}^{3}\delta_i' M_\gamma(-\theta_i'\tau^2)$
$M-$HQAM [57]	$P_s\approx K_{NN}Q(\sqrt{\xi\gamma})+\frac{2}{3}K_{CNN}Q^2\left(\sqrt{\frac{2\xi\gamma}{3}}\right)-2K_{CNN}Q(\sqrt{\xi\gamma})Q\left(\sqrt{\frac{\xi\gamma}{3}}\right)$	$P_{fading}\approx K_{NN}\sum_{i=1}^{2}\delta_i M_\gamma(-\theta_i\xi)+\frac{2}{3}K_{CNN}\sum_{i=1}^{3}\delta_i' M_\gamma(-\lambda_i\xi)-2K_{CNN}\sum_{i=1}^{4}\rho_i M_\gamma(-\lambda_i'\xi)$

[1] $A_1=4\left(1-\frac{1}{\sqrt{M}}\right),A_2=4\left(1-\frac{1}{\sqrt{M}}\right)^2,B_1=\left(4-\frac{2}{M}-\frac{2}{N}\right),B_2=4\left(1-\frac{1}{M}\right)\left(1-\frac{1}{N}\right),C_1=\left(4-\frac{2}{M}-\frac{2}{N}\right),C_2=\left(4-\frac{4}{M}-\frac{4}{N}+\frac{8}{M\times N}\right),K_{NN}=2\left(3-4M^{-\frac{1}{2}}+M^{-1}\right),K_{CNN}=6\left(1-M^{-\frac{1}{2}}\right)^2\sigma=\sqrt{\frac{3}{M-1}};\psi=\sqrt{\frac{12}{5M\times N-4}};\tau=\sqrt{\frac{96}{31M\times N-32}},\xi=\frac{24}{7M-4},\delta_i=\left[\frac{\alpha_{Mopt}}{2},\frac{\beta_{Mopt}}{2}\right],\theta_i=\left[0.971,0.525\right],\delta_i'=\left[\frac{\alpha_{Mopt}^2}{4},\frac{\beta_{Mopt}^2}{4},\frac{\alpha_{Mopt}\beta_{Mopt}}{2}\right],\theta_i'=\left[1.942,1.05,1.496\right],\lambda_i=[0.6473,1.2946,0.9973],\rho_i=\left[\frac{\alpha_{Mopt}^2}{4},\frac{\alpha_{Mopt}\beta_{Mopt}}{4},\frac{\alpha_{Mopt}\beta_{Mopt}}{4},\frac{\beta_{Mopt}^2}{4}\right],\lambda_i'=[1.2946,1.149,0.8486,0.7]$.

Now, referring to Table 8, we substitute P_{AWGN} of SQAM into (19), yielding

$$P_{fading}=A_1\int_0^\infty Q(\sigma\sqrt{\gamma})p_\gamma(\gamma)d\gamma-A_2\int_0^\infty Q^2(\sigma\sqrt{\gamma})\times p_\gamma(\gamma)d\gamma, \tag{21}$$

Further, on substituting the proposed optimized approximation (14a) in place of the GQF present in (21), the same is reduced to several inner integrals which are of the form of

$$I\approx L_1\int_0^\infty e^{-L_2\gamma}p_\gamma(\gamma)d\gamma, \tag{22}$$

where L_1 and L_2 are merely the constants corresponding to each exponential term present in the inner integrals of (21).

It can be clearly seen that (22) is nothing but the definition of MGF corresponding to a fading distribution [1] which for the $\kappa-\mu$ shadowed fading channel is given as [58]

$$M_\gamma(-s)=\frac{(-\mu)^\mu m^m(1+\kappa)^\mu}{\bar{\gamma}^\mu(\mu\kappa+m)^m}\frac{\left((-s)-\frac{\mu(1+\kappa)}{\bar{\gamma}}\right)^{m-\mu}}{\left((-s)-\frac{\mu(1+\kappa)}{\bar{\gamma}}\frac{m}{\mu\kappa+m}\right)^m}. \tag{23}$$

Hence, in terms of simple MGFs, Eq. (21) can now be written as (18) which completes the proof.

It should be noted that a similar analysis can be done for rest of the digital modulation schemes, as listed in Table 8; and therefore the detailed derivations are not explicitly stated over here. Via Table 8, we have just provided the final SEP expressions of all the other digital modulation schemes. It is also worth noticing that the versatility of the $\kappa-\mu$ shadowed fading channel is due to its ability to represent several popular fading channels by a simple variation of the fading parameters, as shown in Table 9. The parameters of the $\kappa-\mu$ shadowed fading channel are underlined in order to differentiate them from the corresponding parameters of the other fading channels.

TABLE 9. Various classical fading channels as special cases of $\kappa-\mu$ shadowed fading channel [58].

Channels	$\kappa-\mu$ **shadowed parameters** [58]
$\kappa-\mu$ fading	$\underline{\mu}=\mu,\underline{\kappa}=\kappa,\underline{m}\to\infty$
Rician (with fading parameter K)	$\underline{\mu}=1,\underline{\kappa}=K,\underline{m}\to\infty$
Rician shadowed	$\underline{\mu}=1,\underline{\kappa}=K,\underline{m}=m$
Nakagami-m	a) $\underline{\mu}=m,\underline{\kappa}\to 0$ b) $\underline{\mu}=\underline{m}=m$
One sided Gaussian	a) $\underline{\mu}=0.5,\underline{\kappa}\to 0$ b) $\underline{\mu}=\underline{m}=0.5$
Rayleigh	a) $\underline{\mu}=1,\underline{\kappa}\to 0$ b) $\underline{\mu}=\underline{m}=1$
$\eta-\mu$ fading	$\underline{\mu}=2\mu,\underline{\kappa}=\frac{1-\eta}{2\eta},\underline{m}=\mu$
Nakagami-q (Hoyt) fading	$\underline{\mu}=1,\underline{\kappa}=\frac{1-q^2}{2q^2},\underline{m}=0.5$

Fig. 5 illustrates the application of (14a) in the SEP computation of 16-SQAM over a special case of the $\kappa-\mu$ shadowed fading channel: the Nakagami-m fading. Precisely, via Fig. 5(a), we first illustrate the significance of HM of the optimal coefficients over the case when we take their arithmetic mean (AM) and geometric mean (GM) as the percentage MRE reduction is best achieved ($\approx 70\%$) when we take their HM. This justifies the approach of taking HM of all the optimal coefficients. We then plot the RE in the SEP of 16-SQAM against the average SNR, $\bar{\gamma}$ (dB). As evident from Fig. 5(b), the RE in SEP computed using the optimized approximation (14a) outperforms the original SEP calculated via (2a) over the entire considered range of $\bar{\gamma}$, i.e., by using (14a) we have managed to reduce the RE in the SEP approximations quite significantly thereby yielding tighter SEP curves which can be seen via Fig. 5(c). We have also included the exact SEP curve which clearly indicates that the optimized SEP is much tighter as compared to the original SEP. The analytical results are also validated with the help of Monte-Carlo simulations which are in excellent agreement with the optimized SEP.

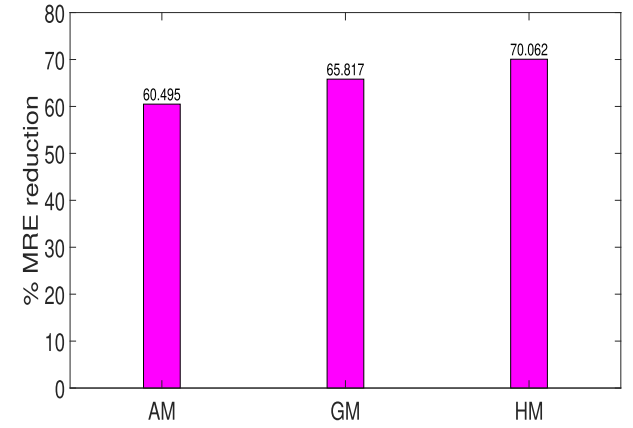

(a)

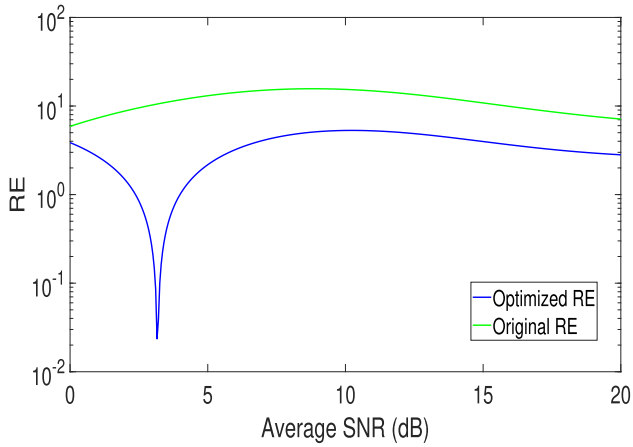

(b)

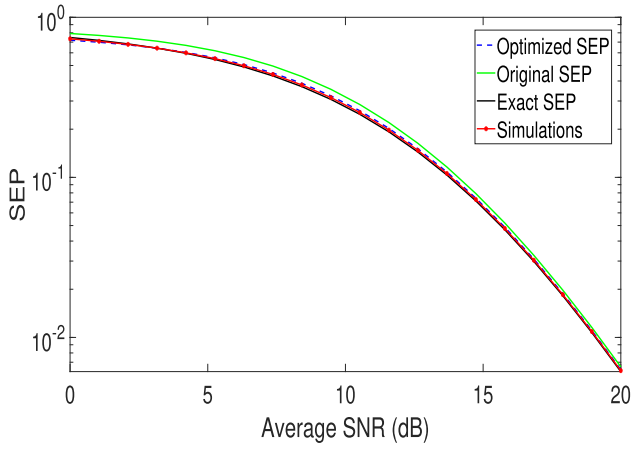

(c)

FIGURE 5. Percentage MRE reduction in 16-SQAM calculated via various types of mean (AM, GM, HM) of the optimized coefficients along with its RE and SEP plots over Nakagami-*m* fading channel ($\mu = 3$; $\kappa = 0$; $m = 3$).

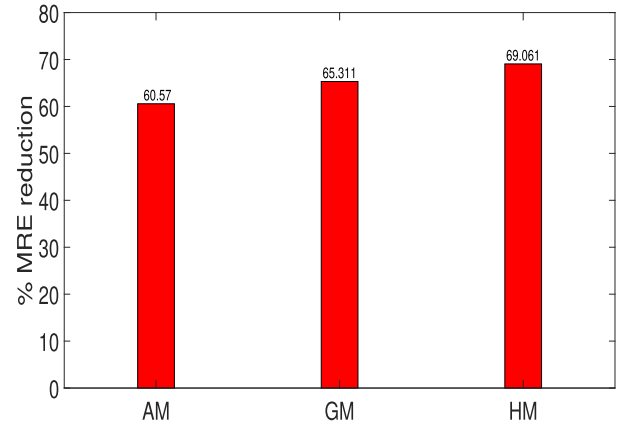

(a)

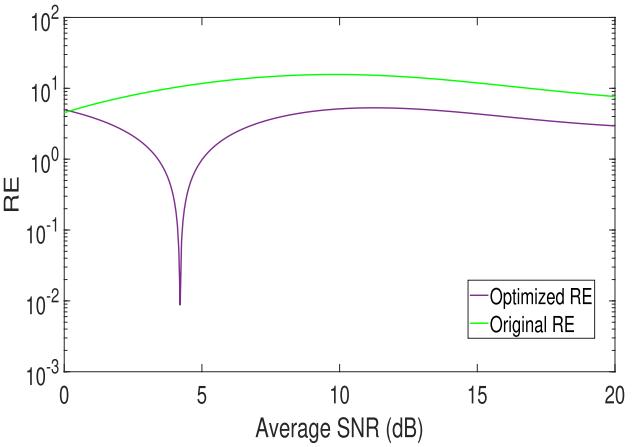

(b)

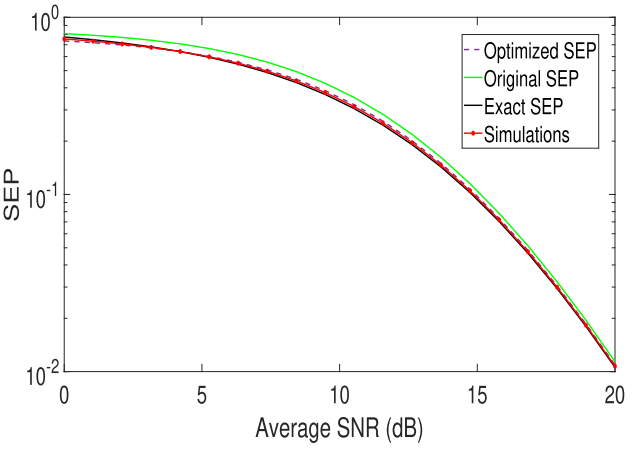

(c)

FIGURE 6. Percentage MRE reduction in 32-RQAM calculated via various types of mean (AM, GM, HM) of the optimized coefficients along with its RE and SEP plots over Nakagami-*m* fading channel ($\mu = 3$; $\kappa = 0$; $m = 3$).

Referring to Fig. 6, we have obtained the similar results for the SEP of another coherent digital modulation technique viz. 32-RQAM. Clearly, here also, the significance of the proposed optimized approximation is quite evident. Hence, in order to avoid any redundancy, we have not explicitly shown the SEP curves for XQAM and HQAM. However, the same can be easily plotted using the derived analytical SEP expressions, as shown in Table 8.

TABLE 10. SEP of 16-SQAM and 32-RQAM computed using original Prony and optimized Prony over Nakagami-m fading channel ($\mu = 3$; $\kappa = 0$; $m = 3$).

16-SQAM					
$\bar{\gamma}$(dB)	0	5	10	15	20
Exact	0.7482	0.5583	0.2768	0.0645	0.0061
Eq. (2a)	0.7923	0.6312	0.3194	0.0715	0.0066
Eq. (14a)	0.7193	0.5704	0.2914	0.0670	0.0063
32-RQAM					
$\bar{\gamma}$(dB)	0	5	10	15	20
Exact	0.7740	0.6067	0.3362	0.0937	0.0106
Eq. (2a)	0.8090	0.6777	0.3888	0.1049	0.0114
Eq. (14a)	0.7354	0.6127	0.3534	0.0978	0.0109

In order to further solidify our analysis, via Table 10, we have provided a numerical comparison of the SEP values obtained from (2a) and (14a) with the exact SEP values. Clearly, for each value of the $\bar{\gamma}$, the values obtained from (14a) are much more closer to the exact SEP values, in comparison to the ones obtained from (2a). Thus, we have made the original Prony-approximation (2) much tighter whilst keeping its simplicity intact.

Noteworthy, the applications of the optimized approximation (14a) are not just limited to performance analysis of the aforementioned digital modulation schemes. Infact, the newly derived optimized parameters can act as one-to-one replacements in several cutting-edge research applications of the original approximation (2a). It should also be noted that since the proposed vector-based IPA is generic in nature, other simple exponential based approximations can also be optimized using the same methodology which further provides an insight on several other applications of all such approximations, vital in communication theory. The applications of these approximations are extensively illustrated in the introduction section and are therefore not stated in this section.

IV. CONCLUSION

Using vector-based IPA, we optimized an already existing simple exponential based approximation of the GQF and computed new optimized coefficients which played a key role in improving the accuracy of the original approximation; for the entire performance range of the GQF. With the help of graphical as well as numerical comparisons, we have illustrated the significance of the proposed optimized approximation. Moreover, the utility of the proposed optimized approximation is also shown by computing the SEP of various coherent digital modulation schemes over a generic and very useful $\kappa - \mu$ shadowed fading channel.

APPENDIX A
PROOF OF LEMMA 1

There are two objectives that $D_{n\times 1}$ must fulfill

1) New data point $Y^{(1)}$ obtained by travelling along the descent direction D must lie inside the FR, i.e., $Y^{(1)}$ represents an interior-point.
2) Travelling along the descent direction must result in the reduction of the cost function value, i.e., $f(Y^{(1)}) < f(Y^{(0)})$.

In order to fulfill the objective (i), it is necessary that the new data point represented by vector $Y^{(1)}$ satisfies the given scaled equality constraints in (8), i.e.,

$$KY^{(1)} = B$$

Using (9), we can rewrite this as

$$KY^{(0)} + \lambda KD = B$$

Now as $Y^{(0)}$ itself is an interior point of the FR, i.e., it satisfies the scaled constraints and so we have $KY^{(0)} = B$. Using this we get $\lambda KD = 0$. Since, $\lambda > 0$ it implies that $KD = 0$ must hold true in order to satisfy objective (i).

By substituting (12) we get $K(-HP) = 0$ and using (10) we get

$$K\left(I - K^T\left(KK^T\right)^{-1}K\right)(-P) = 0$$

Upon further simplifications, it can be shown that this expression will reduce down to $(K-K)(-P) = 0$ which is always true and hence objective (i) is met.

To ensure that objective (ii) is met we first define it in a mathematical form as

$$f\left(Y^{(1)}\right) < f\left(Y^{(0)}\right)$$

and from (7) we can rewrite it as

$$P^T Y^{(1)} < P^T Y^{(0)}$$

By substituting $Y^{(1)}$ as given in (9) we get

$$P^T\left(Y^{(0)} + \lambda D\right) < P^T Y^{(0)}$$

Upon further simplification the above reduces down to yield

$$\lambda P^T D < 0$$

But we know $\lambda > 0$ thus it implies that $P^T D < 0$. This is the condition which has to be met in order to satisfy objective (ii). Now from (12) we can say that

$$P^T D = P^T(-HP)$$

or equivalently

$$P^T D = -P^T HP$$

By using (11b) we can rewrite this as

$$P^T D = -P^T HHP$$

Further by using (11a) we will obtain

$$P^T D = -(HP)^T HP$$

The above expression yields $P^T D = -\|HP\|^2$ and since $\|HP\|^2 > 0$ it implies that $P^T D < 0$ which means our objective (ii) is met. Hence, the definition of D given in (12) is justified.

APPENDIX B
PROOF OF LEMMA 2

We know that

$$Y^{(1)} = Y^{(0)} + \lambda D$$

Thus for any j^{th} element of these vectors we can write

$$y_j^{(1)} = y_j^{(0)} + \lambda d_j$$

Now we know that since $Y^{(0)}$ vector composes of n feasible variables of the FR implying that $y_j^{(0)} \geq 0, \forall j \in [1, n]$. Moreover, the value of $\lambda > 0$ as well. Hence for the vector $Y^{(1)}$ to compose of all feasible variables its imperative that $y_j^{(1)} \geq 0, \forall j \in [1, n]$. However this actually depends on what is the sign and magnitude of d_j. Thus, there are two possible scenarios here:

- If $d_j \geq 0$ then surely we get $y_j^{(1)} \geq 0$ always.
- If $d_j < 0$ then we cannot necessarily say that $y_j^{(1)}$ will always be a positive quantity.

Hence we need to fix some finite value for λ which will ensure that $y_j^{(1)} \geq 0$ holds true, even if $d_j < 0$. So we will now analyse the $d_j < 0$ scenario.

Our objective here is to ensure that

$$y_j^{(1)} \geq 0$$

or equivalently

$$y_j^{(0)} + \lambda d_j \geq 0$$

On multiplying both sides by -1 we get

$$-y_j^{(0)} - \lambda d_j \leq 0$$

which on rearranging yields

$$\lambda \leq \frac{y_j^{(0)}}{-d_j}$$

This implies that the step size λ does have an upper bound to it. Furthermore, the right hand side of the above inequality is a positive quantity as $d_j < 0$. On this basis we now define a parameter λ_{max} as

$$\lambda_{max} = \min_{\forall d_j < 0} \left\{ \frac{y_j^{(0)}}{-d_j} \right\}$$

If we take $\lambda = \lambda_{max}$ directly then it is possible that the new data point vector $Y^{(1)}$ has at least one of its corresponding elements equal to zero which would mean that the IPA had skipped the entire FR and had arrived at one of the boundary points and thus it would nullify our analysis. So instead we choose $\lambda = 0.9 \times \lambda_{max}$ in order to avoid this problem.

REFERENCES

[1] M. K. Simon and M.-S. Alouini, *Digital Communication Over Fading Channels*, 2nd ed. Hoboken, NJ, USA: Wiley, 2005.

[2] M. Chiani, D. Dardari, and M. K. Simon, "New exponential bounds and approximations for the computation of error probability in fading channels," *IEEE Trans. Wireless Commun.*, vol. 2, no. 4, pp. 840–845, Jul. 2003.

[3] P. Loskot and N. C. Beaulieu, "Prony and polynomial approximations for evaluation of the average probability of error over slow-fading channels," *IEEE Trans. Veh. Technol.*, vol. 58, no. 3, pp. 1269–1280, Mar. 2009.

[4] G. K. Karagiannidis and A. S. Lioumpas, "An improved approximation for the Gaussian *Q*-function," *IEEE Commun. Lett.*, vol. 11, no. 8, pp. 644–646, Aug. 2007.

[5] O. Olabiyi and A. Annamalai, "Invertible exponential-type approximations for the Gaussian probability integral $Q(x)$ with applications," *IEEE Wireless Commun. Lett.*, vol. 1, no. 5, pp. 544–547, Oct. 2012.

[6] Y. Isukapalli and B. D. Rao, "An analytically tractable approximation for the Gaussian *Q*-function," *IEEE Commun. Lett.*, vol. 12, no. 9, pp. 669–671, Sep. 2008.

[7] S.-H. Chang, P. C. Cosman, and L. B. Milstein, "Chernoff-type bounds for the Gaussian error function," *IEEE Trans. Commun.*, vol. 59, no. 11, pp. 2939–2944, Nov. 2011.

[8] G. Abreu, "Very simple tight bounds on the *Q*-function," *IEEE Trans. Commun.*, vol. 60, no. 9, pp. 2415–2420, Sep. 2012.

[9] M. López-Benítez and F. Casadevall, "Versatile, accurate, and analytically tractable approximation for the Gaussian *Q*-function," *IEEE Trans. Commun.*, vol. 59, no. 4, pp. 917–922, Apr. 2011.

[10] D. Sadhwani, R. N. Yadav, and S. Aggarwal, "Tighter bounds on the Gaussian *Q* function and its application in Nakagami$-m$ fading channel," *IEEE Wireless Commun. Lett.*, vol. 6, no. 5, pp. 574–577, Oct. 2017.

[11] I. M. Tanash and T. Riihonen, "Global minimax approximations and bounds for the Gaussian *Q*-function by sums of exponentials," *IEEE Trans. Commun.*, vol. 68, no. 10, pp. 6514–6524, Oct. 2020.

[12] I. M. Tanash and T. Riihonen, "Quadrature-based exponential-type approximations for the Gaussian *Q*-function," in *Proc. IEEE 93rd Veh. Technol. Conf. (VTC-Spring)*, Apr. 2021, pp. 1–5.

[13] D. Sadhwani, A. Powari, and N. Mehta, "New, simple and accurate approximation for the Gaussian *Q* function with applications," *IEEE Commun. Lett.*, vol. 26, no. 3, pp. 518–522, Mar. 2022.

[14] I. M. Tanash and T. Riihonen, "Improved coefficients for the Karagiannidis–Lioumpas approximations and bounds to the Gaussian *Q*-function," *IEEE Commun. Lett.*, vol. 25, no. 5, pp. 1468–1471, May 2021.

[15] I. M. Tanash and T. Riihonen, "Generalized Karagiannidis–Lioumpas approximations and bounds to the Gaussian *Q*-function with optimized coefficients," *IEEE Commun. Lett.*, vol. 26, no. 3, pp. 513–517, Mar. 2022.

[16] K.-H. Lee, J. S. Yeom, J. Joung, and B. C. Jung, "Performance analysis of uplink NOMA with constellation–rotated STLC for IoT networks," *IEEE Open J. Commun. Soc.*, vol. 3, pp. 705–717, 2022.

[17] S. Jain, R. Mitra, O. Krejcar, J. Nebhen, and V. Bhatia, "Kernel recursive maximum Versoria criterion based post-distorter for VLC using kernel-width sampling," *IEEE Photon. J.*, vol. 14, no. 3, pp. 1–12, Jun. 2022.

[18] W. Deng, Y. Xia, Z. Li, and W. Pei, "On the distribution of SINR for widely linear MMSE MIMO systems with rectilinear or quasi-rectilinear signals," *IEEE Trans. Veh. Technol.*, vol. 71, no. 2, pp. 1643–1655, Feb. 2022.

[19] M. H. Dinan, N. S. Perović, and M. F. Flanagan, "Sparse layered MIMO with iterative detection," *IEEE Trans. Commun.*, vol. 70, no. 3, pp. 2042–2056, Mar. 2022.

[20] L. Lin, B. Liu, X. Zheng, and Y. Xiao, "An efficient image categorization method with insufficient training samples," *IEEE Trans. Cybern.*, vol. 52, no. 5, pp. 3244–3260, May 2022.

[21] R. C. Ferreira, M. S. P. Facina, F. A. P. De Figueiredo, G. Fraidenraich, and E. R. De Lima, "Bit error probability for large intelligent surfaces under double-Nakagami fading channels," *IEEE Open J. Commun. Soc.*, vol. 1, pp. 750–759, 2020.

[22] L. Zhang, X. Lei, Y. Xiao, and T. Ma, "Large intelligent surface-based generalized index modulation," *IEEE Commun. Lett.*, vol. 25, no. 12, pp. 3965–3969, Dec. 2021.

[23] T. Mao, Q. Wang, Z. Wang, and S. Chen, "Novel index modulation techniques: A survey," *IEEE Commun. Surveys Tuts.*, vol. 21, no. 1, pp. 315–348, 1st Quart., 2019.
[24] L. Xiao, S. Li, Y. Qian, D. Chen, and T. Jiang, "An overview of OTFS for Internet of Things: Concepts, benefits, and challenges," *IEEE Internet Things J.*, vol. 9, no. 10, pp. 7596–7618, May 2022.
[25] T. Lu, J. Ge, Y. Yang, and Y. Gao, "BEP analysis for DF cooperative systems combined with signal space diversity," *IEEE Commun. Lett.*, vol. 16, no. 4, pp. 486–489, Apr. 2012.
[26] M. K. Arti, "Two-way satellite relaying with estimated channel gains," *IEEE Trans. Commun.*, vol. 64, no. 7, pp. 2808–2820, Jul. 2016.
[27] M. R. Bhatnagar, Z. Ghassemlooy, S. Zvanovec, M.-A. Khalighi, and M. M. Abadi, "Quantized feedback-based differential signaling for free-space optical communication system," *IEEE Trans. Commun.*, vol. 64, no. 12, pp. 5176–5188, Dec. 2016.
[28] A. Garg, M. R. Bhatnagar, O. Berder, and B. Vrigneau, "Quantized feedback-based diagonal precoding for $N \times 1$ MISO system with generalized orthogonal space-time block codes," *IEEE Trans. Commun.*, vol. 66, no. 1, pp. 91–104, Jan. 2018.
[29] X. Yu, W. Xu, S.-H. Leung, and J. Wang, "Unified performance analysis of transmit antenna selection with OSTBC and imperfect CSI over Nakagami- *m* fading channels," *IEEE Trans. Veh. Technol.*, vol. 67, no. 1, pp. 494–508, Jan. 2018.
[30] A. Garg, M. R. Bhatnagar, O. Berder, and B. Vrigneau, "Performance analysis of erroneous feedback-based MIMO system over Nakagami-*m* fading channels," *IEEE Trans. Commun.*, vol. 67, no. 8, pp. 5403–5418, Aug. 2019.
[31] I. Trigui, W. Ajib, W.-P. Zhu, and M. D. Renzo, "Performance evaluation and diversity analysis of RIS-assisted communications over generalized fading channels in the presence of phase noise," *IEEE Open J. Commun. Soc.*, vol. 3, pp. 593–607, 2022.
[32] A. Sikri, A. Mathur, and G. Kaddoum, "Signal space diversity-based distributed RIS-aided dual-hop mixed RF-FSO systems," *IEEE Commun. Lett.*, vol. 26, no. 5, pp. 1066–1070, May 2022.
[33] X. Zhang, Z. Chen, Y. Xu, Y. Zhu, and X. Wang, "PoM: Power-efficient multi-view video streaming over multi-antenna wireless systems," *IEEE Trans. Green Commun. Netw.*, vol. 3, no. 4, pp. 919–932, Dec. 2019.
[34] R. Cai, Q. Tian, and T. Qiu, "A low complexity DOA estimation method of CD sources in impulsive noise," *IEEE Access*, vol. 9, pp. 142857–142868, 2021.
[35] D. Sadhwani, "Simple and tightly approximated integrals over κ-μ shadowed fading channel with applications," *IEEE Trans. Veh. Technol.*, vol. 67, no. 10, pp. 10092–10096, Oct. 2018.
[36] Y. Mouchtak and F. E. Bouanani, "New accurate approximation for average error probability," *IEEE Access*, vol. 9, pp. 4388–4397, 2021.
[37] P. K. Singya, P. Shaik, N. Kumar, V. Bhatia, and M.-S. Alouini, "A survey on higher-order QAM constellations: Technical challenges, recent advances, and future trends," *IEEE Open J. Commun. Soc.*, vol. 2, pp. 617–655, 2021.
[38] I. M. Tanash and T. Riihonen, "Remez exchange algorithm for approximating powers of the $Q-$ function by exponential sums," in *Proc. IEEE 93rd Veh. Technol. Conf. (VTC-Spring)*, 2021, pp. 1–6.
[39] J. Zhang, X. Li, I. S. Ansari, Y. Liu, and K. A. Qaraqe, "Performance analysis of dual-hop satellite relaying over κ-μ shadowed fading channels," in *Proc. IEEE Wireless Commun. Netw. Conf.*, Mar. 2017, pp. 1–6.
[40] S. Kumar, "Approximate outage probability and capacity for κ-μ shadowed fading," *IEEE Wireless Commun. Lett.*, vol. 4, no. 3, pp. 301–304, Jun. 2015.
[41] S. L. Cotton, "Human body shadowing in cellular device-to-device communications: Channel modeling using the shadowed κ-μ fading model," *IEEE J. Sel. Areas Commun.*, vol. 33, no. 1, pp. 111–119, Jan. 2015.
[42] F. J. Cañete *et al.*, "Measurement and modeling of narrowband channels for ultrasonic underwater communications," *Sensors*, vol. 16, no. 2, pp. 1–12, Feb. 2016.
[43] S. Kumar and S. Kalyani, "Outage probability and rate for κ-μ shadowed fading in interference limited scenario," *IEEE Trans. Wireless Commun.*, vol. 16, no. 12, pp. 8289–8304, Dec. 2017.
[44] J. Zhang, X. Chen, K. P. Peppas, X. Li, and Y. Liu, "On high-order capacity statistics of spectrum aggregation systems over κ-μ and κ-μ shadowed fading channels," *IEEE Trans. Commun.*, vol. 65, no. 2, pp. 935–944, Feb. 2017.
[45] X. Li, J. Li, L. Li, J. Jin, J. Zhang, and D. Zhang, "Effective rate of MISO systems over κ-μ shadowed fading channels," *IEEE Access*, vol. 5, pp. 10605–10611, 2017.
[46] S. Parthasarathy and R. K. Ganti, "Coverage analysis in downlink poisson cellular network with κ-μ shadowed fading," *IEEE Wireless Commun. Lett.*, vol. 6, no. 1, pp. 10–13, Feb. 2017.
[47] Y. J. Chun, S. L. Cotton, H. S. Dhillon, F. J. Lopez-Martinez, J. F. Paris, and S. K. Yoo, "A comprehensive analysis of 5G heterogeneous cellular systems operating over κ-μ shadowed fading channels," *IEEE Trans. Wireless Commun.*, vol. 16, no. 11, pp. 6995–7010, Nov. 2017.
[48] G. Chandrasekran and S. Kalyani, "Performance analysis of cooperative spectrum sensing over κ-μ shadowed fading," *IEEE Wireless Commun. Lett.*, vol. 4, no. 5, pp. 553–556, Oct. 2015.
[49] J. Zhang, L. Dai, W. H. Gerstacker, and Z. Wang, "Effective capacity of communication systems over κ-μ and κ-μ shadowed fading channels," *IET Electron. Lett.*, vol. 51, no. 19, pp. 1540–1542, Sep. 2015.
[50] M. R. Bhatnagar, "On the sum of correlated squared κ-μ shadowed random variables and its application to performance analysis of MRC," *IEEE Trans. Veh. Technol.*, vol. 64, no. 6, pp. 2678–2684, Jun. 2015.
[51] S. L. Cotton, "Shadowed fading in body-to-body communications channels in an outdoor environment at 2.45 GHz," in *Proc. IEEE-APS Topical Conf. Antennas Propag. Wireless Commun.*, Aug. 2014, pp. 249–252.
[52] Q. Shi and Y. Karasawa, "An accurate and efficient approximation to the Gaussian *Q*-function and its applications in performance analysis in Nakagami-*m* fading," *IEEE Commun. Lett.*, vol. 15, no. 5, pp. 479–481, May 2011.
[53] Y. Mouchtak and F. E. Bouanani, "New tighter upper bounds on the performance of convolutional code over exponentially correlated rayleigh fading channel," in *Proc. IEEE Int. Wireless Commun. Mobile Comput. Conf. (IWCMC)*, Sep. 2016, pp. 863–868.
[54] W. M. Jang, "A simple upper bound of the Gaussian *Q*-function with closed-form error bound," *IEEE Commun. Lett.*, vol. 15, no. 2, pp. 157–159, Feb. 2011.
[55] F. E. Bouanani, Y. Mouchtak, and G. K. Karagiannidis, "New tight bounds for the Gaussian *Q*-function and applications," *IEEE Access*, vol. 8, pp. 145037–145055, 2020.
[56] D. Sadhwani and R. N. Yadav, "A simplified exact expression of SEP for cross QAM in AWGN channel from M×N rectangular QAM and its usefulness in Nakagami-*m* fading channel," *AEU Int. J. Electron. Commun.*, vol. 74, pp. 63–74, Apr. 2017.
[57] L. Rugini, "Symbol error probability of hexagonal QAM," *IEEE Commun. Lett.*, vol. 20, no. 8, pp. 1523–1526, Aug. 2016.
[58] J. F. Paris, "Statistical characterization of $\kappa-\mu$ shadowed fading," *IEEE Trans. Veh. Technol.*, vol. 63, no. 2, pp. 518–526, Feb. 2014.
[59] I. S. Gradshteyn and I. M. Ryzhik, *Table of Integrals, Series, and Products*, 7th ed. New York, NY, USA: Academic, 1980.

ADITYA POWARI is currently pursuing the B.Tech. degree in electrical engineering and is associated with the Department of Electrical and Computer Science Engineering, Institute of Infrastructure Technology Research and Management, Ahmedabad. He has worked as a Research Intern with the Department of Electrical and Computer Engineering, National University of Singapore and with the Department of Electrical Engineering, Indian Institute of Technology Delhi, New Delhi. His research interests span over the fields of wireless communications, information theory, optical communications, and digital signal processing.

DHARMENDRA SADHWANI received the B.Tech. degree in electronics and communication engineering from the University Institute of Technology Bhopal, India, in 2007, the M.Tech. and Ph.D. degrees in wireless communication from the Maulana Azad National Institute of Technology (formerly MACT), Bhopal, India, in 2013 and 2018, respectively. In 2019, he joined the Department of Electrical and Computer Science Engineering, Institute of Infrastructure Technology Research and Management, Ahmedabad, India, where he is currently an Assistant Professor. His research interests include application of Gaussian Q function in communication theory, error performance analysis and identification of more efficient higher order digital modulation schemes, statistical characterization of fading channels, satellite communication systems, 5G communications, cooperative communication systems, under water acoustics (systems), Poisson's cellular networks, body to body communications, shadowing in communication systems, and application of machine learning/neural networks in communication theory.

LALITA GUPTA (Senior Member, IEEE) received the B.E. degree in electronics and telecommunication engineering from Pt. Ravi Shankar Shukla University, Raipur, in 2003, and the M.Tech. degree in digital communication and the Ph.D. degree in electronics and communications engineering from the Maulana Azad National Institute of Technology, Bhopal, India, in 2007 and 2012, respectively. Since July 2004, she has been associated as a Faculty Member with the Maulana Azad National Institute of Technology, where she is currently an Associate Professor with the Department of Electronics and Communication Engineering. She has 30 research publications in various international journals and conference of repute. Her research interests include signal processing and image processing. She is a member of IETE and ICEIT.

RAM NARAYAN YADAV received the B.Tech. degree in electronics from the Motilal Nehru National Institute of Technology (formerly MNREC) Allahabad, India, in 1993, the M.Tech. degree in digital communication from the Maulana Azad National Institute of Technology (formerly MACT), Bhopal, India, in 1997, and the Ph.D. degree in electrical engineering from IIT Kanpur, India, in 2005. In 1997, he joined the Department of Electronics and Communication Engineering, Maulana Azad National Institute of Technology, where he is currently a Professor. He has published more than 70 articles in various international journals and conferences, including journals of IEEE, IET, Elsevier, and Springer. He has supervised 25 masters and ten doctoral students. His current research interests include communication systems, image processing, and neural networks and applications. He is also a reviewer of several IEEE and Elsevier journals.